ResearchGate

See discussions, stats, and author profiles for this publication at: https://www.researchgate.net/publication/5570173

Synthesis of Electromagnetic Functionalized Barium Ferrite Nanoparticles Embedded in Polypyrrole

ARTICLE *in* THE JOURNAL OF PHYSICAL CHEMISTRY B · APRIL 2008

Impact Factor: 3.3 · DOI: 10.1021/jp710259v · Source: PubMed

CITATIONS
54

READS
113

7 AUTHORS, INCLUDING:

Ping Xu
Harbin Institute of Technology
101 PUBLICATIONS **2,926** CITATIONS
SEE PROFILE

Hongtao Zhao
12 PUBLICATIONS **171** CITATIONS
SEE PROFILE

Jingyu Wang
Huazhong University of Science and Technol…
29 PUBLICATIONS **610** CITATIONS
SEE PROFILE

Available from: Ping Xu
Retrieved on: 26 January 2016

ARTICLES

Synthesis of Electromagnetic Functionalized Barium Ferrite Nanoparticles Embedded in Polypyrrole

Ping Xu,[†] Xijiang Han,*[,†] Chao Wang,[†] Hongtao Zhao,[†] Jingyu Wang,[†] Xiaohong Wang,[‡] and Bin Zhang[†]

Department of Applied Chemistry, Harbin Institute of Technology, Harbin 150001, China, and Beijing Institute of Aeronautical Materials, Beijing 100095, China

Received: October 24, 2007; In Final Form: December 19, 2007

With flaky $BaFe_{12}O_{19}$ nanoparticles (BF NPs, 10−20 nm in thickness) as polymerization seeds, electromagnetic functionalized and microstructured quasi-spherical PPY/BF (PPY: polypyrrole) organic−inorganic composites were prepared by a conventional in situ chemical oxidative polymerization. X-ray diffraction and Fourier transform infrared analyses interpreted that there was no obvious chemical interaction between BF NPs and PPY in the composites but that BF NPs only served as the nucleation sites for the polymerization of pyrrole. As compared to pure BF NPs, PPY/BF composites showed distinct increases in electrical conductivities and decreases in magnetization and thus improved the matched characteristic impedance of the free space, leading to a substantial enhancement of reflection loss at 2−18 GHz. For the first time, multi-layered and single-layered films formed at different places on the reaction flask were studied by scanning electron microscopy and energy dispersive X-ray analysis, indicating that the films composed of quasi-spherical microstructures can be very different in morphology but surprisingly contain no BF NPs.

Introduction

Organic−inorganic composites with an organized structure usually provide a new functional hybrid, with synergetic or complementary behavior between organic and inorganic materials, which have attracted considerable attention for their potential applications. In recent years, there has been a tremendous increase in interest in materials that are both magnetic and electrically conductive, which have potential applications such as electromagnetic shielding (EMS), molecular electronics, nonlinear optics, microwave absorption, and catalysis.[1,2] In particular, electrically conductive macromolecules such as polypyrrole (PPY) and polyaniline (PANI) containing metal oxide nanoparticles (NPs)[3−6] and metal NPs[7−13] have been prepared and investigated for different applications. Among those multi-functionalized micro-/nanostructures, electromagnetic functionalized micro-/nanostructures of conducting polymers are of special interest due to their potential applications in EMS and microwave absorbing materials. Recently, a few articles on the electromagnetic functional micro-/nanostructures of conducting polymers have been published.[14−16] PPY is known as one of the most important conducting polymers due to its high conductivity, ease of preparation, and good environmental stability, and the embedment of NP cores inside the conducting PPY is of interest because of the strong electronic interaction between NPs and polymer matrices.[17,18]

It was demonstrated that electrical conductivities are intrinsic to the conducting polymers, while their magnetic properties are induced by magnetic materials in the composites.[19] The molecular structure of the electrical and magnetic component in micro-/nanostructured composites affects the electromagnetic properties of the micro-/nanostructured composites. In our previous work, by supplying $BaFe_{12}O_{19}$ (BF) NPs as nucleation sites, the produced PANI/BF nanocomposites have alternative electrical conductivities and magnetic properties.[20] It was found that PANI coating on BF NPs substantially reinforced the reflection loss of barium ferrite at 2−18 GHz. Moreover, microwave absorbing properties can be modulated simply by controlling the thickness of the samples for the required frequency bands.

In this study, selecting PPY as the conducting polymer, electromagnetic functionalized PPY/BF microstructured composites were prepared by a conventional in situ chemical oxidative polymerization, with HCl as the dopant and ammonium persulfate (APS) as the oxidant. It was understood that the content of the inorganic phase can significantly affect the morphology and electrical, magnetic, and electromagnetic properties of the resulting PPY/BF composites. For the first time, to our knowledge, the morphologies and chemical compositions of the formed films at different places on the flask were investigated by SEM and EDX, which revealed that the films can be multi-layered or single-layered but conformably contain no BF NPs.

Experimental Procedures

Synthesis of BF NPs and PPY/BF Composites. $BaFe_{12}O_{19}$ NPs were prepared by a reverse microemulsion technique as

* Corresponding author. Tel.: +86-451-86413702; fax: +86-451-86418750; e-mail: pingxu_hit@yahoo.com.cn.
[†] Harbin Institute of Technology.
[‡] Beijing Institute of Aeronautical Materials.

10.1021/jp710259v CCC: $40.75 © 2008 American Chemical Society
Published on Web 02/19/2008

reported in a previous work.[21] The PPY/BF composites were synthesized by in situ chemical oxidative polymerization in the presence of BF NPs, with APS as the oxidant and HCl as the dopant. A typical preparation process for PPY/BF composites is as follows: BF NPs were added to 0.2 M HCl under ultrasonication for 30 min to obtain a uniform suspension, and then the pyrrole monomer was added under ultrasonication for another 30 min to form a pyrrole/HCl mixture containing BF. The mixture was cooled in an ice−water bath for 1 h before a precooled APS aqueous solution was added for oxidative polymerization for 24 h under vigorous mechanical stirring, with the temperature controlled at 0−5 °C. The precipitated powder was centrifuged and washed with distilled water and anhydrous ethanol until the filtrate became colorless and then was dried in a vacuum drying cabinet at 80 °C for 24 h. Throughout the experiment, the molar ratio of pyrrole to HCl ([pyrrole]/[HCl]) and to APS ([pyrrole]/[APS]) was retained at 1:1. Effects of the concentration of BF NPs on the morphology, structure, and physicochemical properties of the resulting PPY/BF composites were studied by modulating mass ratios of the pyrrole monomer to BF NPs at 2:1, 4:1, 9:1, and 19:1 respectively. Pure PPY was prepared under the same conditions without the inorganic NPs.

Characterization. Scanning electron microscopy (SEM) measurements were carried out on the FEI Serion scanning microscope to study the morphology of the samples, and the samples were mounted on aluminum studs using adhesive graphite tape and were sputter-coated with gold before analysis. The chemical composition was measured by energy dispersive X-ray analysis (EDX) (EDAX− Inc.). The characteristics of the crystallite structure of the prepared samples were determined using an XRD-6000 X-ray diffractometer (Shimadzu) with a Cu Kα radiation source ($\lambda = 1.5405$ Å, 40.0 kV, and 30.0 mA). Fourier transform infrared (FT-IR) spectroscopy was measured on a Nicolet Avatar 360 FT-IR spectrometric analyzer with KBr pellets. The electrical conductivity of compressed rods at room temperature was measured by a standard four-probe method using a Keithley 2400 System digital source meter. The surface areas of the resulting products were measured by nitrogen adsorption−desorption isotherms using the Brunauer−Emmett−Teller (BET) method (Quantachrome, Autosorb-1). The samples were degassed under vacuum at 100 °C before measurement. The magnetic properties (intrinsic coercivity, saturation, and remanent magnetization) were measured using a vibrating sample magnetometer (VSM, Lake Shore 7307). A HP-5783E vector network analyzer was applied to determine the relative permeability and permittivity in the frequency range of 2−18 GHz for the calculation of reflection loss. A sample containing 50 wt % obtained products was pressed into a ring with an outer diameter of 7 mm, an inner diameter of 3 mm, and a thickness of 2 mm for microwave measurement, in which paraffin wax was used as the binder.

Results and Discussion

The SEM image of the prepared PPY powders from a conventional chemical oxidative polymerization shows typical granular (quasi-spherical) morphologies (Figure 1a), with an average diameter of about 0.8 μm. PPY powders containing BF NPs also displayed quasi-spherical structures (Figure 1b−e), while it was discovered that with an increase in the content of BF NPs, the average diameters of the produced composite powders were gradually reduced. As stated, PPY powders with a nanofibrillar morphology can be observed in systems in which the seed template must (i) itself possess a nanofibrillar morphology and (ii) also be capable of oxidatively reacting with the pyrrole monomer.[22] No fibrillar morphology was observed when passive or inert seed templates were used; therefore, by supplying flaky and inert BF NPs prepared from a reverse microemulsion technique as polymerization seeds (10−20 nm thickness, Figure 1f), the intrinsic granular morphology of PPY prepared in an aqueous phase was not influenced. With a low content of BF NPs, the particle sizes of the produced PPY/BF composites were not changed obviously (Figure 1b,c), as compared to the pure PPY powders. However, growth of PPY at the surfaces of BF NPs will consume a considerable amount of pyrrole monomer with a further increase in the content of the inorganic NPs, and the growth of the particle size can be restrained to some extent; thus, composites with smaller grain sizes are obtained (Figure 1d,e). EDX spectra of the samples confirm the existence of BF NPs in the formed quasi-spherical structures. As we found from Figure 1e (white circles), flaky structures can be distinguished from the synthesis of PPY/BF composites from a mass ratio of pyrrole monomer/BF NPs of 2:1. An EDX study of this sample shows that the flaky structures are mainly composed of BF NPs, while the spherical structures are PPY powders containing BF NPs. We believe that continuing to increase the content of BF NPs will produce samples with more flaky structures, as we found in a previous work that only flaky structures can be obtained with a high content (90 wt %) of the inorganic phase during the preparation of PANI/BF nanocomposites, rather than coralloid structures with directional nanofibers obtained at lower contents of BF NPs.[21] Fundamental differences between the PPY and the PANI systems require different kinds of seed templates to ensure fibrillar polymer growth. The fibrillar growth is intrinsic to polyaniline, and the added seed template directs the synthetic trajectory along these pre-existing pathways.[23,24] In the PPY system, however, these pathways have to be induced, by using either seed templates that are intrinsically reactive toward the pyrrole monomer or those that can be rendered reactive by treatment with APS.[22] Thus, with the inert BF NPs as the seed templates, only quasi-spherical structures were obtained for the PPY/BF composites.

Different from the preparation of PANI/BF nanocomposites, obvious and thick films were formed at the side-neck and on the wall of the three-necked flask in the preparation of both pure PPY and PPY/BF composites (which can be manually separated from the flask), and it was discovered that the formed film at the side-neck was much thicker than that on the wall. Further investigation of the film at the side-neck indicated that it is multi-layered and can be delaminated into more layers manually. The SEM image of the uppermost layer of the formed multi-layered film in the preparation of PPY/BF composites from a mass ratio of pyrrole monomer and BF NPs of 4:1 is shown in Figure 2. Unlike the dispersed granular particles in the prepared powders as shown in Figure 1, the uppermost layer of the formed multi-layered film consists of rod-like microstructures (Figure 2a); we believe that the formation of such structures is closely related to the nonhomogeneous effect of mechanical stirring at the side-neck during the synthesis process. Partial magnification of the layer reveals that the rod-like microstructures are 4−5 μm in diameter and are composed of overlapping granular particles with nearly identical sizes to the prepared PPY powders. Surprisingly, the elemental composition analysis of the uppermost layer by EDX in Figure 2c indicates the nonexistence of Ba and Fe elements from BF NPs, and the detected element S can be attributed to the produced SO_4^{2-} ions from the reduction of APS and partial doping by H_2SO_4 of the polymer chains or the surface adsorbed unreacted APS. SEM

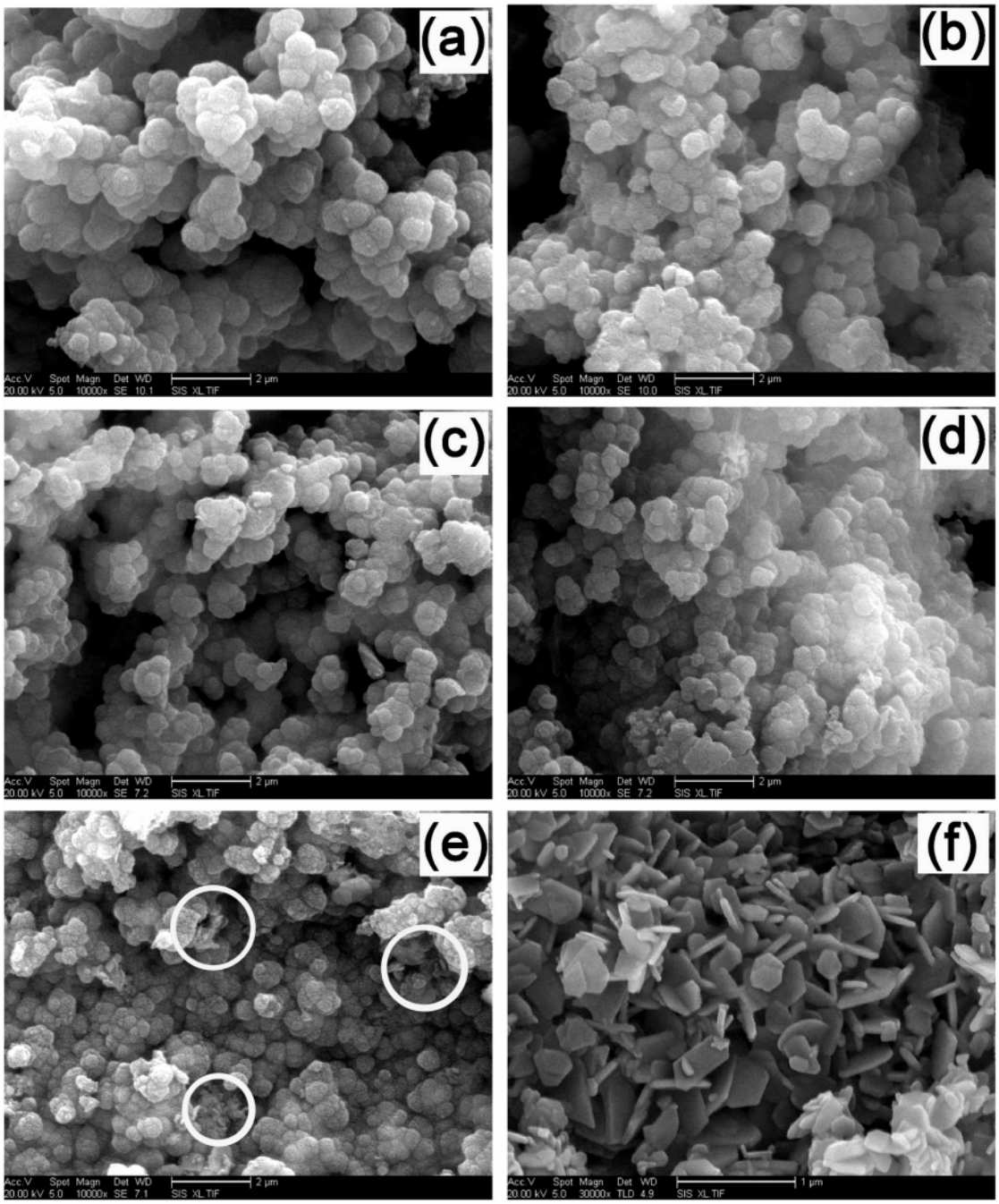

Figure 1. SEM images of (a) pure PPY, PPY/BF composites synthesized from different mass ratios of pyrrole monomer and BF NPs at (b) 19:1, (c) 9:1, (d) 4:1, (e) 2:1, by an in situ oxidative polymerization method, and (f) BF NPs prepared from a reverse microemulsion technique.

images of the following layers of the formed multi-layered film in Figure 3 show that these layers are denser films with obvious holes. From the manually delaminated three layers and EDX analysis, we found that each layer was also composed of granular PPY particles, and from layer 1 to layer 3 (Figure 3b−d), the film becomes much denser, and the composed particles and holes become smaller, which may be interpreted that the polymerization of the pyrrole monomer proceeds layer by layer and that the coverage of a new layer would restrain the particle growth of the old layer(s); thus, denser films were produced in lower layers. The holes in the middle layers of the multi-layered films may be caused by the impulsive force of the liquid phase; however, the mechanism responsible for the formation of holes during the preparation of both PPY and PPY/BF composites remains to be elucidated. From the designated frame on layer 2 in Figure 3a, it can be found that layer 2 itself consists of several thin layers; thus, a further study of each layer of the formed multi-layered films could be carried out for a deep understanding of the formation mechanism of such films.

The film formed on the wall of the flask was determined to be single-layered and cannot be delaminated manually, and Figure 4 shows the SEM images of the film surface toward the reaction solution and adhered to the wall. As seen in Figure 4a,c, the film was so thin that corrugation was found on both surfaces due to the impulsive force of the liquid phase during the reaction process, which shows greatly different morphologies to the films formed at the side-neck. As for the film surface toward the reaction solution, magnification of the formed ridges reveals that the surface was constructed by uniform spherical particles (Figure 4b), with an average diameter of about 0.75

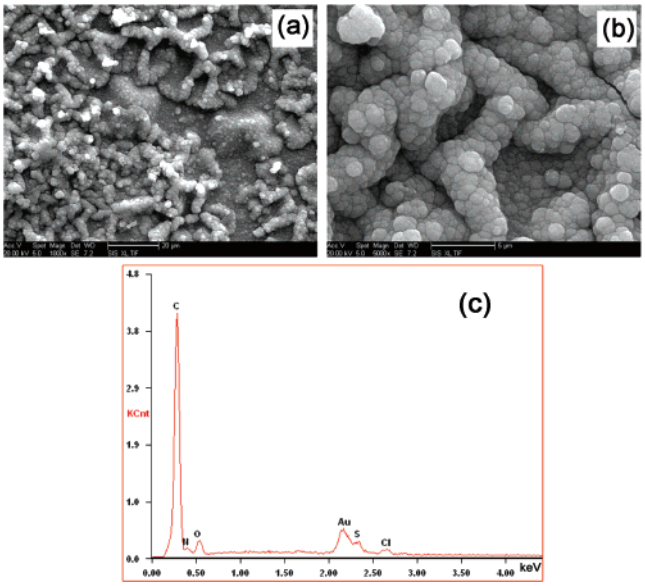

Figure 2. SEM images of (a) uppermost layer of the formed film at the side-neck of the three-necked flask in preparation of PPY/BF composites from a mass ratio of pyrrole monomer and BF NPs at 4:1 and (b) partial magnification of panel a. (c) EDX analysis from panel b, where no Ba and Fe elements were detected.

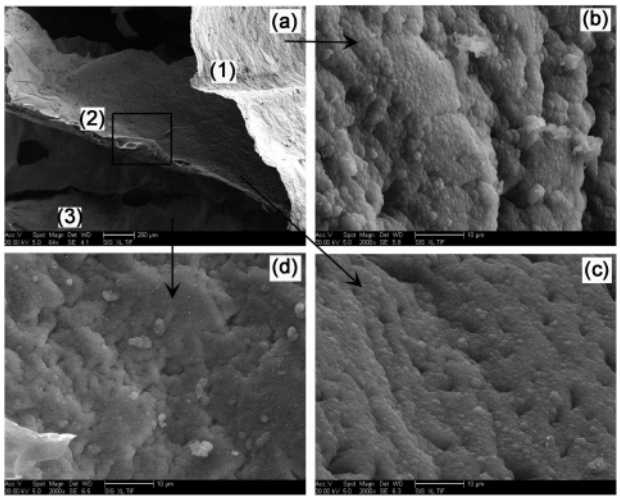

Figure 3. SEM images of the following layers of the formed film at the side-neck of the three-necked flask in preparation of PPY/BF composites synthesized from a mass ratio of pyrrole monomer and BF NPs at 4:1. Partial magnification of each layer is also given.

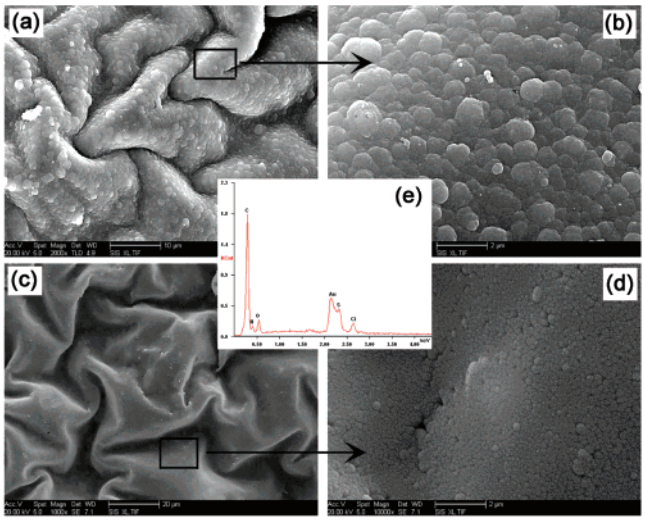

Figure 4. SEM images of (a) the surface toward the reaction solution of the film formed at the wall of the three-necked flask in preparation of PPY/BF composites synthesized from a mass ratio of pyrrole monomer and BF NPs at 4:1; (b) partial magnification of panel a; (c) the surface adhered to the flask wall of the formed film; (d) partial magnification of panel c; and (e) EDX analysis of the formed film, where no Ba and Fe elements were detected.

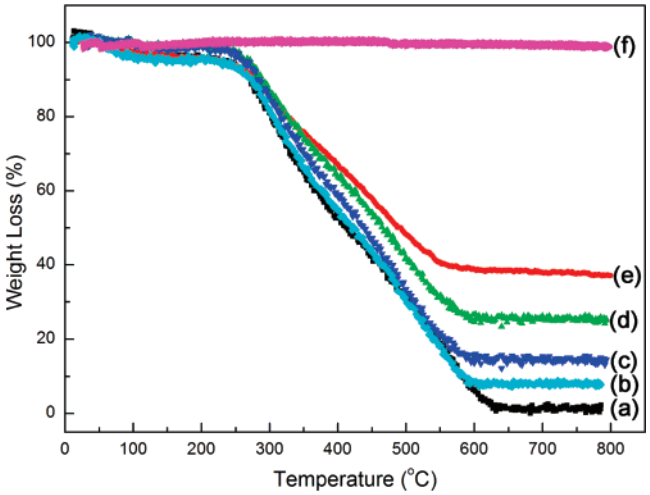

Figure 5. Thermogravimetric curves of the prepared (a) pure PPY, PPY/BF composites synthesized from different mass ratios of pyrrole monomer and BF NPs at (b) 19:1, (c) 9:1, (d) 4:1, (e) 2:1, and (f) BF NPs from room temperature to 800 °C.

μm. While from the magnification of the surface adhered to the wall (Figure 4d), it was discovered that this surface was very smooth, with no obvious stereoscopic morphology, instead, the spherical particles were embedded in the film to give a flat surface. The growth of the particles was greatly restrained on this surface because the diameters of the spherical particles were in the range of 150−200 nm. The same as the elemental composition of the film formed at the side-neck, EDX analysis also shows no Ba and Fe elements from BF NPs in the film at the wall (Figure 4e). Therefore, we believe that during the polymerization of pyrrole, PPY can be directly formed with the glass mediate as polymerization seeds, with the intrinsic spherical morphologies unchanged. To reduce or avoid the PPY formation on the flask, surface decoration of the glass mediate may be required (e.g., the addition of some surfactant).

Since PPY can grow at the glass mediate and the formed films contain no BF NPs, it is unambiguous that the mass ratios of PPY and BF of the obtained PPY/BF composites should not follow the designed values. From the thermogravimetric (TG) curves (room temperature to 800 °C) of the prepared pure PPY and PPY/BF composites shown in Figure 5, two weight loss regions were discovered for all samples, due to the removal of surface absorbed water and the combustion of PPY. Pure PPY can be completely combusted, and BF NPs are stable and will not suffer from weight loss during this TG analysis; thus, the content of BF NPs in PPY/BF composites can be calculated as

$$\text{BF wt \%} = \frac{1 - L_{\text{total}}}{1 - L_{\text{water}}} \times 100\% \qquad (1)$$

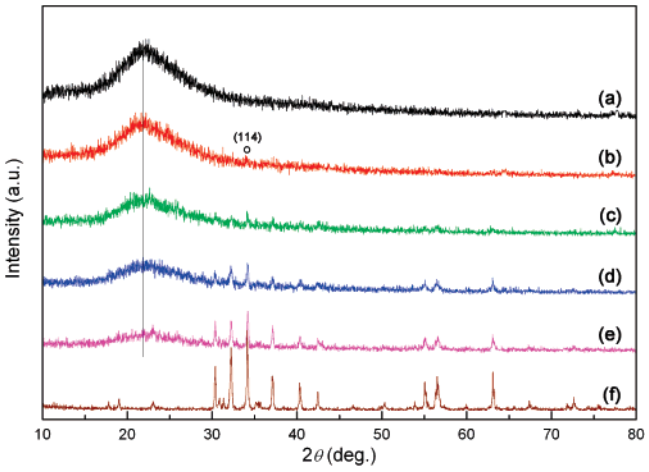

Figure 6. X-ray diffraction patterns of (a) pure PPY, (b) PPY−8.1 wt % BF, (c) PPY−13.5 wt % BF, (d) PPY−24.7 wt % BF, (e) PPY−38.2 wt % BF, and (f) pure BF NPs.

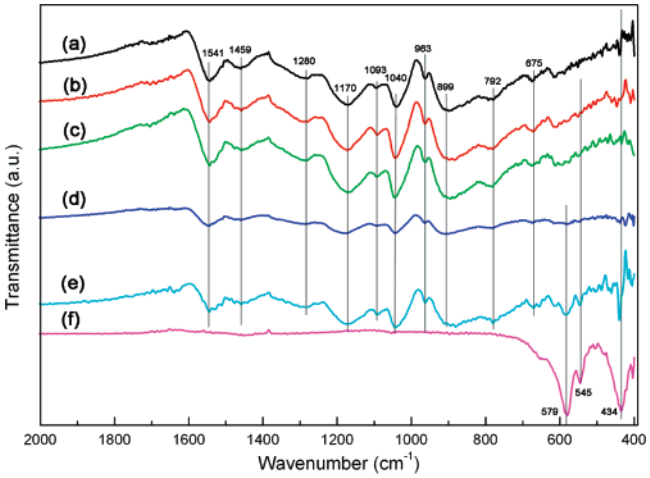

Figure 7. FT-IR spectra of (a) pure PPY, (b) PPY−8.1 wt % BF, (c) PPY−13.5 wt % BF, (d) PPY−24.7 wt % BF, (e) PPY−38.2 wt % BF, and (f) pure BF NPs.

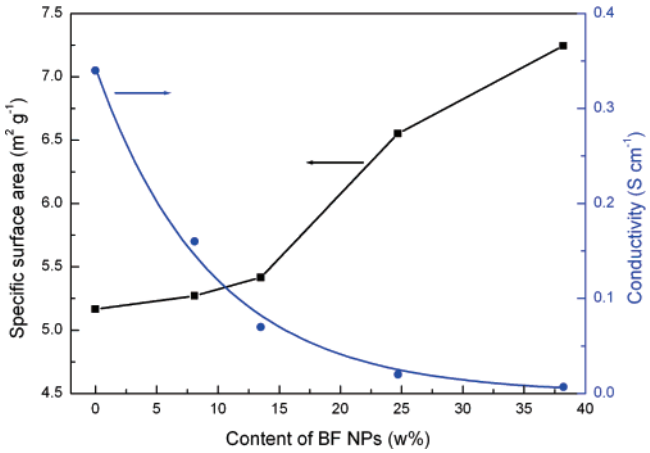

Figure 8. Effect of BF concentration on the room-temperature electrical conductivities and specific surface areas of the prepared PPY and PPY/BF composites.

where L_{total} and L_{water} are the total weight loss and weight loss from water, respectively. It was calculated that the real contents of BF NPs in the PPY/BF composites synthesized from designed mass ratios of pyrrole monomer and BF NPs at 2:1, 4:1, 9:1, and 19:1 were 38.2, 24.7, 13.5, and 8.1 wt %, respectively. As expected, the contents of BF NPs are a little bit higher in PPY/BF composites than the designed composites; thus, a slight overdose of the pyrrole monomer is needed for accurately controlling the core/shell mass ratio during the preparation of PPY composites.

Figure 6 shows the X-ray diffraction (XRD) patterns for the prepared PPY, PPY/BF composites, and BF NPs. In Figure 6a, the XRD pattern of protonated PPY exhibits a broad amorphous diffraction peak at approximately the $2\theta = 18-27°$ range. This broad peak is centered at around $2\theta = 23°$, corresponding to the scattering from bare polymer chains at the interplanar spacing.[25,26] Generally, X-ray scattering provides information about the structure of polymer chains and their spatial order at atomic dimensions. It has been reported that the structure of polypyrroles doped with common inorganic counterions is essentially amorphous. Moreover, it is well-known that during the chemical synthesis of PPY, $\alpha-\alpha'$ bonds are predominantly formed, but a small proportion of $\alpha-\beta$ bonds are also present, leading to structural disorder (branching, cross-links), hence resulting in an amorphous PPY.[27] It is clear that PPY/BF composites (Figure 6b−e) combined both the diffraction peaks from pure BF NPs (Figure 6f, JCPDS no. 27−1029) and the broad peak from protonated PPY with somewhat a change in the intensity. As shown, with the increase in the content of BF NPs in PPY/BF composites, the broad amorphous diffraction peak of PPY becomes weaker, while the diffraction peaks corresponding to BF become more distinguishable and stronger. For the 8.1 wt % BF embedded PPY, only the diffraction peak referring to the (114) plane of BF can be recognized.

FT-IR spectra of the prepared protonated PPY, PPY/BF composites, and pure BF NPs are displayed in Figure 7. For protonated PPY (Figure 7a), the bands observed at 1541 and 1459 cm^{-1} relate to the fundamental vibrations of the pyrrole rings.[28] The broad band from 1400 to 1250 cm^{-1} is attributed to the =C−H in-plane deformation modes, with a maximum at 1280 cm^{-1}. In the region of the C−N stretching vibrations from 1250 to 1100 cm^{-1}, one can observe a maximum at 1170 cm^{-1} in the spectra. The peak observed at 1093 cm^{-1} corresponds to the in-plane deformation vibration of NH^+, which is formed on the PPY chains by protonation.[29] The bands corresponding to the C−H and N−H in-plane deformation vibrations were situated at 1040 cm^{-1} and to the C−C out-of-plane ring deformation vibration at 963 cm^{-1}.[30] The region of the C−H out-of-plane deformation vibration of the ring is located at 899 cm^{-1}, and the C−H out-of-plane ring deformation vibration is located at 792 cm^{-1}.[29] The peak at 675 cm^{-1} refers to the C−C out-of-plane ring deformation vibration or to the C−H rocking vibration.[27] The FT-IR spectrum of the prepared BF NPs (Figure 7f), with peaks at 579, 545, and 434 cm^{-1}, indicates the formation of pure barium ferrite, without the band corresponding to $BaFe_2O_4$ at 765 cm^{-1}.[31] The as-prepared PPY/BF composites (Figure 7b−e) not only have characteristic vibrations for protonated PPY, but also those corresponding to the prepared BF NPs. Moreover, it can be discovered that the characteristic vibrational peaks found for PPY/BF composites almost have no shifts as compared to those for protonated PPY and BF NPs. XRD and FT-IR analyses may indicate that there is no obvious chemical interaction between BF NPs and PPY in the composites[3,16] but that BF NPs only serve as the nucleation sites for the polymerization of pyrrole.

As shown in Figure 8, higher BET− specific surface areas were discovered for PPY/BF composites as compared to pure PPY powders. With an increase in the content of BF NPs, the specific surface areas were increased slightly, which may originate from the decrease in the average particle sizes of the

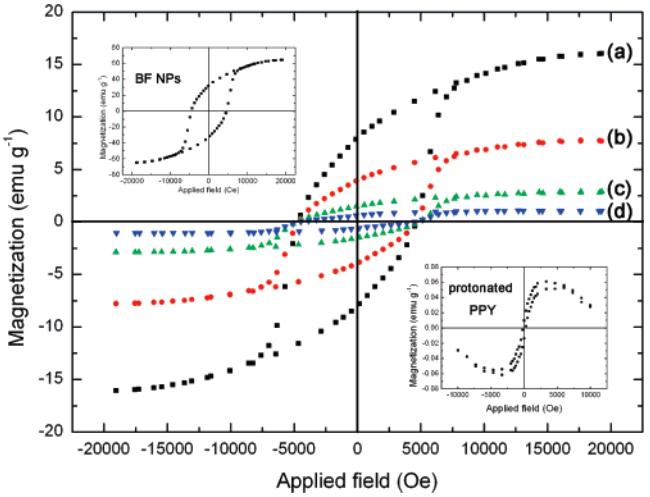

Figure 9. Room-temperature field-dependent magnetization curves of (a) PPY−38.2 wt % BF, (b) PPY−24.7 wt % BF, (c) PPY−13.5 wt % BF, (d) PPY−8.1 wt % BF, BF NPs, and protonated PPY (inset).

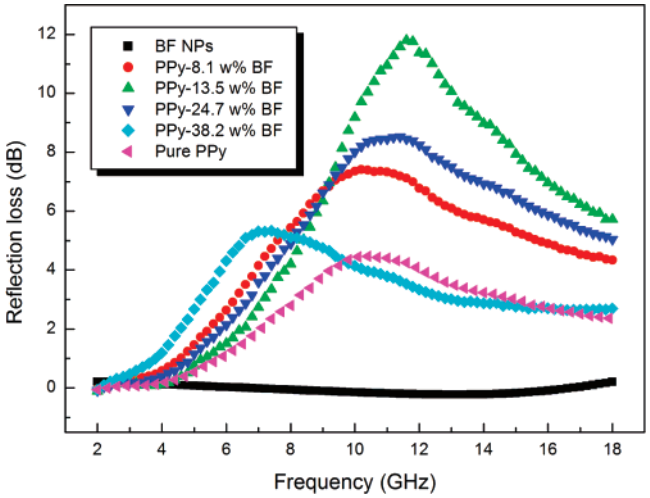

Figure 10. Reflection loss for PPY/BF composites, pure PPY powders, and BF NPs, with a sample thickness of 2 mm in the frequency range of 2−18 GHz. In measurements, the 50 wt % sample and 50 wt % paraffin wax were used.

produced quasi-spherical structures. Electrical conductivities of PPY/BF composites have a first-order exponential decay relationship as a function of the content of BF NPs due to the reduction in the doping degree of PPY and the insulating behavior of BF (Figure 8); however, the conductivities are 4−5 orders of magnitude larger than that of BF NPs ($\approx 10^{-6}$ S cm^{-1}) and still comparable to some reported PPY micro-/nanocomposites.[32,33] An increase in charge carrier scattering from the embedment of BF NPs in the PPY matrix, and an increased charge carrier trapping, either by the NPs themselves or by morphological change and defects induced by them, both lead to an increase in resistivity.[15] In other words, electrical conductivity of the BF NPs can be enhanced by the conductive PPY coating. It is well-known that the surface chemistry greatly affects the magnetic properties of fine magnetic particles due to their relatively larger surface area,[34] and as shown in Figure 9, coercivities of PPY/BF composites decrease slightly as compared to BF NPs, due to the reduction in surface anisotropy upon coating,[35,36] but are qualitatively larger than that of PPY, resulting in the production of hard magnetic materials. However, coating of PPY on BF NPs significantly reduces the saturation ($\boldsymbol{M}_S$) and remanent ($\boldsymbol{M}_R$) magnetization value, due to the dominant diamagnetic nature of PPY (Figure 9, inset). Magnetization exhibits monotone increasing functions with the content of BF NPs in the PPY/BF composites (1.04, 2.90, 7.71, and 16.06 emu g^{-1} for 8.1, 13.5, 24.7, and 38.2 wt % BF embedded PPY), indicating that the magnetic properties of the composites are induced by the magnetic materials. The ratio of remanent magnetization and saturation magnetization, $\boldsymbol{M}_R/\boldsymbol{M}_S$ for the prepared BF NPs is very close to 0.5, indicating that $BaFe_{12}O_{19}$ crystals of a single magnetic domain were synthesized.[37] It was interestingly discovered that PPY coating retained the single magnetic domain characteristic of BF NPs since values of $\boldsymbol{M}_R/\boldsymbol{M}_S$ for all prepared PPY/BF composites were still close to 0.5. Magnetic properties are strongly dependent on the particle size as well as the crystalline structure and the chemical bonding at the surface.[8] As the observed magnetic properties of fine particles are a combination of many anisotropy mechanisms, the PPY coating on the BF NPs will likely affect the contributions of the surface anisotropy, shape anisotropy, and interface anisotropy to the net anisotropy. Therefore, in the polymerization of pyrrole with BF NPs as the nucleation sites, hard magnetic materials with controllable conductivities and magnetic properties can be produced.

The normalized input impedance Z_{in} of a metal-backed microwave-absorbing layer is given by[38−40]

$$Z_{in} = \sqrt{\frac{\mu_r}{\epsilon_r}} \tanh\left[j\left(\frac{2\pi}{c}\right)\sqrt{\mu_r \epsilon_r} f d\right] \qquad (2)$$

where μ_r and ϵ_r are the relative permeability and permittivity, respectively, of the composite medium, c is the velocity of electromagnetic waves in free space, f is the frequency of microwaves, and d is the thickness of the absorber. The reflection loss is related to Z_{in} as

$$R\ (\mathrm{dB}) = 20 \log\left|\frac{Z_{in} - 1}{Z_{in} + 1}\right| \qquad (3)$$

Figure 10 shows the reflection loss of the prepared PPY/BF composites, pure PPY powders, and BF NPs (50 wt % sample plus 50 wt % paraffin wax) with a thickness of 2 mm in the frequency range of 2−18 GHz, which demonstrates that the reflection loss characteristics are sensitive to the content of BF NPs. PPY also has some microwave absorption at 2−18 GHz due to its dielectric loss. The reflection loss toward the electromagnetic waves of the PPY/BF composites was enhanced substantially, as compared to that of pure BF NPs, which exhibited hardly any microwave absorption at 2−18 GHz for their resonance frequency located at 47.6 GHz.[41,42] The frequency relating to maximum reflection loss can be modulated by altering the content of BF NPs, and the increased reflection loss at a higher frequency range was accompanied by the attenuation at lower frequency bands. Among all the samples, the PPY/BF composite containing 13.5 wt % of BF NPs had the largest reflection loss of 11.8 dB at 11.6 GHz. At a relatively smaller thickness (2 mm), the reflection loss properties of the PPY/BF composites were superior or comparable to some conducting polymer composites.[43,44] For the PPY/BF composite with 38.2 wt % BF, a better reflection loss property was found only between 2 and 10 GHz as compared to PPY, indicating that the presence of BF NPs uncovered by PPY is detrimental to the composite performance, which complies with the finding that the mixtures of PANI and BF NPs have poorer reflection loss properties than the corresponding PANI/BF composites.[20]

Besides the complex relative permeability μ_r and permittivity ϵ_r, another important parameter relating to reflection loss is the concept of matched characteristic impedance, where the characteristic impedance of the absorbing material should be made nearly equal to that of the free space to achieve zero reflection at the front surface of the material.[45] PPY can be regarded as a dielectric loss material for its high permittivity ϵ_r,[46,47] and the increase in magnetic properties and decrease in electrical conductivity of PPY/BF composites as compared to PPY powders are expected to improve the matched characteristic impedance of the free space, thus finally leading to a better reflection loss. Besides the morphological diversity, the fundamental differences between PANI and PPY may also lead to variable reflection loss properties of the prepared composites. On the whole, conducting polymers with proper magnetic properties may be applied as a kind of microwave absorption material in gigahertz frequency.

Conclusion

Conventional in situ chemical oxidative polymerization allowed the preparation of microstructured quasi-spherical and electromagnetic functionalized PPY/BF organic−inorganic composites, with flaky BF NPs as nucleation cites, and no evident chemical interactions were discovered between PPY and BF NPs. The content of BF NPs can strongly affect the morphologies and physicochemical properties of the prepared composites. By comparison with pure BF NPs, the PPY/BF composites show an enhanced electrical conductivity, weakened magnetic property, and improved matched characteristic impedance of free space, resulting in reinforced reflection loss properties at 2−18 GHz. The formation of multi-layered and single-layered films without containing BF NPs on the reaction flask increased the content of BF NPs in the composites more than in the designed composites; thus, a slight overdose of the pyrrole monomer is needed for the preparation of PPY composites with an accurate control of the core/shell mass ratio.

Acknowledgment. P.X. thanks advanced engineers Xinrong Liu, Zushun Lv, Xuandong Li, and Aihua Wen for helpful discussions. This work was supported by the NSF of China (20676024 and 20776032) and the Innovative Foundation of Heilongjiang Academy of Sciences (HKXY-CX-07001-03).

Supporting Information Available: Additional EDX spectra. This material is available free of charge via the Internet at http://pubs.acs.org.

References and Notes

(1) Gomez-Romero, P. *Adv. Mater.* **2001**, *13*, 163.

(2) Wuang, S. C.; Neoh, K. G.; Kang, E. T.; Pack, D. W.; Leckband, D. E. *J. Mater. Chem.* **2007**, *17*, 3354.

(3) Zhang, L.; Wan, M. *J. Phys. Chem. B* **2003**, *107*, 6748.

(4) Hosono, K.; Matsubara, I.; Murayama, N.; Woosuck, S.; Izu, N. *Chem. Mater.* **2005**, *17*, 349.

(5) Chowdhury, D.; Paul, A.; Chattopadhyay, A. *Langmuir* **2005**, *21*, 4123.

(6) Qiu, G.; Wang, Q.; Nie, M. *Macromol. Mater. Eng.* **2006**, *291*, 68.

(7) Sawall, D. D.; Villahermosa, R. M.; Lipeles, R. A.; Hopkins, A. R. *Chem. Mater.* **2004**, *16*, 1606.

(8) Watanabe, N.; Morais, J.; Accione, S. B. B.; Morrone, Â.; Schmidt, J. E.; Martins Alves, M. C. *J. Phys. Chem. B* **2004**, *108*, 4013.

(9) Tseng, R. J.; Huang, J.; Ouyang, J.; Kaner, R. B.; Yang Y. *Nano Lett.* **2005**, *5*, 1077.

(10) Pillalamarri, S. K.; Blum, F. D.; Tokuhiro, A. T.; Bertino, M. F. *Chem. Mater.* **2005**, *17*, 5941.

(11) Chen, A.; Wang, H.; Li, X. *Chem. Commun. (Cambridge, U.K.)* **2005**, 1863.

(12) Feng, X.; Huang, H.; Ye, Q.; Zhu, J.; Hou, W. *J. Phys. Chem. C* **2007**, *111*, 8463.

(13) Herrasti, P.; del Rio, A. I.; Recio, J. *Electrochim. Acta* **2007**, *52*, 6496.

(14) Yoon, M.; Kim, Y.; Kim, Y. M.; Yoon, H.; Volkov, V.; Avilov, A.; Park, Y. J.; Park, I. W. *J. Magn. Magn. Mater.* **2004**, *272*−*276*, 1259.

(15) Long, Y. Z.; Chen, Z. J.; Duvail, J. L.; Zhang, Z. M.; Wan, M. X. *Physica B* **2005**, *370*, 121.

(16) Li, X.; Wan, M.; Wei, Y.; Shen, J.; Chen, Z. *J. Phys. Chem. B* **2006**, *110*, 14623.

(17) Selvan, S. T.; Spatz, J. P.; Klok, H.; Möller, M. *Adv. Mater.* **1998**, *10*, 132.

(18) Tian, S.; Liu, J.; Zhu, T.; Knoll, W. *Chem. Mater.* **2004**, *16*, 4103.

(19) Wan, M. X.; Li, J. C. *Synth. Met.* **1999**, *101*, 844.

(20) Xu, P.; Han, X.; Jiang, J.; Wang, X.; Li, X.; Wen, A. *J. Phys. Chem. C* **2007**, *111*, 12603.

(21) Xu, P.; Han, X.; Wang, M. *J. Phys. Chem. C* **2007**, *111*, 5866.

(22) Zhang, X.; Manohar, S. K. *J. Am. Chem. Soc.* **2004**, *126*, 12714.

(23) Zhang, X.; Goux, W. J.; Manohar, S. K. *J. Am. Chem. Soc.* **2004**, *126*, 4502.

(24) Huang, J.; Kaner, R. B. *J. Am. Chem. Soc.* **2004**, *126*, 851.

(25) Ouyang, J.; Li, Y. *Polymer* **1997**, *38*, 3997.

(26) Seo, I.; Pyo, M.; Cho, G. *Langmuir* **2002**, *18*, 7253.

(27) Karim, M. R.; Lee, C. J.; Lee, M. S. *Polym. Adv. Technol.* **2007**, in press.

(28) Nguyen, T.; Diaz, A. *Adv. Mater.* **1994**, *6*, 858.

(29) Blinova, N. V.; Stejskal, J.; Trchová, M.; Proke×f0, J.; Omastová, M. *Eur. Polym. J.* **2007**, *43*, 2331.

(30) ×bben, S.; Gök, A.; Gülce, H. *J. Appl. Polym. Sci.* **2007**, *106*, 3852.

(31) Huang, J. G.; Zhuang, H. R.; Li, W. L. *Mater. Res. Bull.* **2003**, *38*, 149.

(32) Murugendrappa, M. V.; Prasad, M. V. N. A. *J. Appl. Polym. Sci.* **2007**, *103*, 2797.

(33) Liu, J.; Wan, M. *J. Polym. Sci., Part A: Polym. Chem.* **2000**, *38*, 2734.

(34) Yavuz, Ö.; Ram, M. K.; Aldissi, M.; Poddar, P.; Hariharan, S. *J. Mater. Chem.* **2005**, *15*, 810.

(35) Vestal, C. R.; Zhang, Z. J. *J. Am. Chem. Soc.* **2003**, *125*, 9828.

(36) Vestal, C. R.; Zhang, Z. J. *Nano Lett.* **2003**, *3*, 1739.

(37) Yu, H. F.; Huang, K. C. *J. Magn. Magn. Mater.* **2003**, *260*, 455.

(38) Singh, P.; Babbar, V. K.; Razdan, A.; Puri, R. K.; Goel, T. C. *J. Appl. Phys.* **2000**, *87*, 4362.

(39) Park, K.; Lee, S.; Kim, C.; Han, J. *Comput. Sci. Technol.* **2006**, *66*, 576.

(40) Zhu, H.; Lin, H.; Guo, H.; Yu, L. *Mater. Sci. Eng., B* **2007**, *138*, 101.

(41) Kagotani, T.; Fujiwara, D.; Sugimoto, S.; Inomata, K.; Homma, M. *J. Magn. Magn. Mater.* **2004**, *272*−*276*, 1813.

(42) Qiu, J.; Zhang, Q.; Gu, M. *J. Appl. Phys.* **2005**, *98*, 103905.

(43) Abbas, S. M.; Dixit, A. K.; Chatterjee, R.; Geol, T. C. *Mater. Sci. Eng., B* **2005**, *123*, 167.

(44) Martins, C. R.; Faez, R.; Rezende, M. C.; De Paoli, M. A. *Polym. Bull.* **2004**, *51*, 321.

(45) Vinoy, K. J.; Jha, R. M. *Radar Absorbing Materials: From Theory to Design and Characterization*; Kluwer Academic Publishers: Dordrecht, The Netherlands, 1996.

(46) Saafan, S. A.; El-Nimr, M. K.; El-Ghazzawy, E. H. *J. Appl. Polym. Sci.* **2006**, *99*, 3370.

(47) Wang, Y.; Jing, X. *Polym. Adv. Technol.* **2005**, *16*, 344.